Cell Death and Differentiation (2014) 21, 864–875
© 2014 Macmillan Publishers Limited All rights reserved 1350-9047/14
www.nature.com/cdd

High sphingomyelin levels induce lysosomal damage and autophagy dysfunction in Niemann Pick disease type A

E Gabandé-Rodríguez[1], P Boya[2], V Labrador[1], CG Dotti[1] and MD Ledesma*[,1]

Niemann Pick disease type A (NPA), which is caused by loss of function mutations in the acid sphingomyelinase (ASM) gene, is a lysosomal storage disorder leading to neurodegeneration. Yet, lysosomal dysfunction and its consequences in the disease are poorly characterized. Here we show that undegraded molecules build up in neurons of acid sphingomyelinase knockout mice and in fibroblasts from NPA patients in which autophagolysosomes accumulate. The latter is not due to alterations in autophagy initiation or autophagosome–lysosome fusion but because of inefficient autophago–lysosomal clearance. This, in turn, can be explained by lysosomal membrane permeabilization leading to cytosolic release of Cathepsin B. High sphingomyelin (SM) levels account for these effects as they can be induced in control cells on addition of the lipid and reverted on SM-lowering strategies in ASM-deficient cells. These results unveil a relevant role for SM in autophagy modulation and characterize autophagy anomalies in NPA, opening new perspectives for therapeutic interventions.
Cell Death and Differentiation (2014) **21,** 864–875; doi:10.1038/cdd.2014.4; published online 31 January 2014

Lysosomal storage disorders (LSDs) are characterized by progressive accumulation of undigested macromolecules within the cell.[1] The impaired degradation of substrates in LSDs is assigned to lysosomal dysfunction. However, recent evidence indicates that deficient degradation in LSDs also derives from alterations in endosomal and autophagosomal pathways, which flow into the lysosomal system.[2]

Autophagy is the process involved in the degradation of cytoplasmic organelles and cytosolic components. The best characterized kind of autophagy, macroautophagy, starts with the formation of an isolation membrane enveloping cytoplasmic cargoes to generate an autophagosome. The autophagosome then fuses with the lysosome to form an autophagolysosome. Cargo degradation takes place in this organelle by specific enzymes.[3,4] Deficiencies in different steps of the autophagic pathway have been recently described in several LSDs.[2] These evidences led to the hypothesis that removal of autophagic buildup could be a suitable approach to treat these diseases. However, these findings also underscored the need to independently define the nature of the autophagy impairment for each LSD. Because lipid storage characterizes many of these disorders, this research effort could also serve to define the poorly understood role of lipids in autophagy.

Sphingolipidoses are LSDs for which autophagy analysis is scarce.[2] Niemann Pick disease type A (NPA) is a sphingolipidosis caused by loss of function mutations in the gene *SMPD1* encoding for the acid sphingomyelinase (ASM).[5] This enzyme catalyzes sphingomyelin (SM) conversion into ceramide in lysosomes.[6] As a result of ASM deficiency, cells from NPA patients accumulate SM in their lysosomes.[7] The disease has a severe neurological involvement that leads to early death.[8] In mice lacking ASM (acid sphingomyelinase knockout mice, ASMko), which are a model for NPA,[9] gradual accumulation of SM occurs in brain lysosomes and at the plasma and synaptic membranes of neurons.[10,11] Here we have analyzed the autophagy–lysosomal systems in the brain of ASMko mouse and in fibroblasts from NPA patients. Our work demonstrates the existence of autophagy alterations in this disease, defines SM excess as a key determinant in these alterations and proposes strategies to revert them.

Results

Autophagy alterations in ASMko mice brains. Neurological signs such as progressive spasticity and motor skill difficulties are among the most characteristic signs of NPA. Consistently, neuronal death in NPA patients and in ASMko mice is particularly evident in the cerebellum.[12] This prompted us to investigate the autophagy/lysosomal system in the cerebellum of mice lacking ASM. Electron microscopy analysis revealed abundant multilamellar bodies and membrane-bound/autophagosome-like structures in the cytoplasm of ASMko Purkinje cells (Figure 1a). This phenotype was already evident at 3 months of age, in agreement with the early storage pathology described in different brain areas of ASMko mice.[12] Immunostaining with the lysosome-associated membrane protein 1 (Lamp1) confirmed the lysosomal nature of enlarged structures (Figure 1b). Western blotting experiments indicated

[1]Centro Biología Molecular Severo Ochoa, CSIC-UAM, Madrid 28049, Spain and [2]Centro Investigaciones Biológicas, CSIC, Madrid 28040, Spain
*Corresponding author: MD Ledesma, Centro Biología Molecular Severo Ochoa, CSIC-UAM, Nicolás Cabrera 1, Madrid 28049, Spain. Tel: +34 911964535; Fax: +34 911962044; E-mail: dledesma@cbm.csic.es
Keywords: sphingomyelin; lysosomal membrane permeabilization; Niemann Pick type A; Cathepsin B; autophagy
Abbreviations: NPA, Niemann Pick type A; ASM, acid sphingomyelinase; SM, sphingomyelin; LSDs, lysosomal storage disorders; ASMko, acid sphingomyelinase knockout mice; FB1, Fumonisin B1; BafA1, Bafilomycin A1; LMP, lysosomal membrane permeabilization
Received 19.7.13; revised 13.12.13; accepted 23.12.13; Edited by H-U Simon; published online 31.1.14

significantly higher levels of the lysosomal marker Lamp2 (Figure 1c) and of the autophagosomal marker LC3-II but not of LC3-I (Figure 1d) in the cerebellum of 3-month-old ASMko mice compared with wt mice (2-fold and 2.4-fold, respectively). The upregulation of these proteins was even greater when 6-month-old mice were analyzed (20-fold and 3.3-fold, respectively).

To determine whether the increased levels of autophagosome proteins such as LC3-II were due to enhancement of the initial steps of autophagy, we measured the levels of the early autophagy markers Atg5-Atg12 complex and Beclin1. Different from LC3-II, the amount of these proteins was similar or slightly decreased in ASMko compared with wt cerebellar extracts (Figures 1e and f).

Altogether, increased autophago–lysosomal volume and upregulation of Lamp2 and LC3-II in the absence of enhanced autophagy initiation suggested that the lysosomal disorder of NPA disease is the consequence of defects in the late steps of degradation.

Impaired protein degradation and increased cell death in ASMko mice brains. To confirm that the ultrastructural, cell biological and biochemical parameters of lysosome–autophagosome anomalies reflected functional alteration, we investigated the degradative capacity in cerebellar neurons from ASMko mice. As autophagy impairment leads to the accumulation of ubiquitinated proteins,[13,14] ubiquitin-positive protein aggregates were analyzed. In agreement with autophago–lysosomal dysfunction, ubiquitin aggregates were abundant in the ASMko neurons compared with wt neurons (Figure 2a). Consistent with the time of LC3-II upregulation, the aggregates were evident in the 3-month-old mice. At 6 months of age, when most Purkinje cells have degenerated, ubiquitin aggregates were also evident in other cell types of the granular layer of ASMko mice cerebellum (Figure 2a). Western blot analysis of ASMko cerebellar extracts confirmed the higher content of ubiquitinated proteins (1.91-fold) (Figure 2b) and of p62 (1.67-fold), which seeds aggregates of ubiquitinated proteins in autophagosomes[15] (Figure 2c). Also increased were the levels of another autophagy adapter protein, NBR1, which is a LC3 and ubiquitin-binding scaffold protein that can function independently of p62 and accumulates when autophagy is impaired[16] (Supplementary Figure 1).

Autophagy interference and accumulation of undegraded material lead to neuronal death.[17,18] We thus sought to determine whether impaired autophagy has a pathological role in the absence of ASM. To this aim we investigated whether neuronal death parallels accumulation of LC3 by immunostaining of the cerebellum with antibodies against LC3 and caspase-cleaved actin (Fractin), which is a feature for apoptosis.[19] Positive cells for Fractin were 6.2-fold more abundant in the ASMko compared with wt cerebellum and matched those accumulating LC3 (Figure 2d). Because impairment of other autophagic pathways such as the chaperone-mediated autophagy could also contribute to cell death, we determined whether this process was altered. Arguing against this possibility, we found no differences in the levels of any of the chaperone-mediated autophagy markers (Hsp90, Hsc70 and Hsp40) analyzed in ASMko compared with wt cerebellum (Supplementary Figure 2).

In all, these data confirm macroautophagy, but not chaperone-mediated autophagy, impairment in the ASMko mice brains. The accumulation of nondegraded autophagic substrates correlating with increased apoptosis in ASMko cells suggests a relevant pathogenic role for deficient autophagy in NPA.

SM addition induces autophagy alterations in wt neurons. It has been proposed that altered lipid content (i.e., high cholesterol or ganglioside levels) may contribute to autophagy impairment.[20–24] On the other hand, the lipid that most significantly accumulates in neurons from ASMko mice is SM.[10] Hence, we directly tested whether SM accumulation was responsible for the autophagosome–lysosome alterations observed in the ASMko mice brain. To this aim, SM was added to cultured primary neurons from wt mice. Lysenin staining[25] indicated 0.85-fold increase of SM levels in the treated neurons, similar to that detected in ASMko neurons,[10] without affecting cell viability (Figure 3a, see also Galvan *et al*.[10]). SM rise resulted in 0.52-fold higher LC3-II levels (Figure 3b) and led to 0.6-fold increase in ubiquitinated proteins (Figure 3c) in wt neurons. These data supported the direct link between autophagosome–lysosome alterations and SM increase in ASM-deficient neurons. Loss of function experiments in ASM-deficient human-derived cells confirmed this conclusion (see below).

Fibroblasts from NPA patients show similar autophagy alterations compared with the ASMko mice brain. Two questions arose from the above results: where along the autophagosome–lysosome pathway is the defect in ASM-deficient cells? How does dysfunction occur? To address these questions, we switched to a cellular system more amenable to experimentation: fibroblasts from NPA patients. These cells could also add relevance to our results in the human scenario. We first sought to confirm that the alterations observed in the ASMko mice cerebellum affected NPA fibroblasts. Electron microscopy indicated bigger areas of multilamellar bodies and membrane-bound structures with cytoplasmic contents consistent with autophagolysosomes in fibroblasts from NPA patients compared with control individuals (Figure 4a). Moreover, the two NPA fibroblast lines analyzed showed increased LC3-II amount (44-fold in average) compared with the two control lines (Figure 4b) but unaltered Atg5-Atg12 complex and Beclin1 (Figures 4c and d) levels. To corroborate that morphological and biochemical alterations were accompanied by dysfunction, we monitored p62 levels and the rate of degradation of the EGF receptor (EGFR), which, on binding of its ligand EGF, is ubiquitinated and sorted for lysosomal degradation.[26] Consistent with deficient autophagy, p62 levels were increased in the NPA fibroblasts (Figure 4e). In agreement with defective lysosomal degradation, the amount of EGFR at 30, 60 and 120 min after EGF stimulation decreased by 15%, 45% and 30%, respectively, in control fibroblasts, whereas in NPA fibroblasts EGFR levels increased 185 and 115% at 30 and 60 min and diminished (by a 27%) only at the latest time monitored after stimulation (120 min) (Figure 4f).

These results confirmed the structural and functional similarities of the autophago–lysosomal defects in ASMko neurons and NPA fibroblasts, and validated the latter as an experimental system to analyze the underlying mechanisms.

Reduction of SM, but not of cholesterol, prevents autophagy alterations. The experiments of SM addition in ASMko neurons indicated a key role for this lipid in autophagy alterations (Figure 3). With the following series

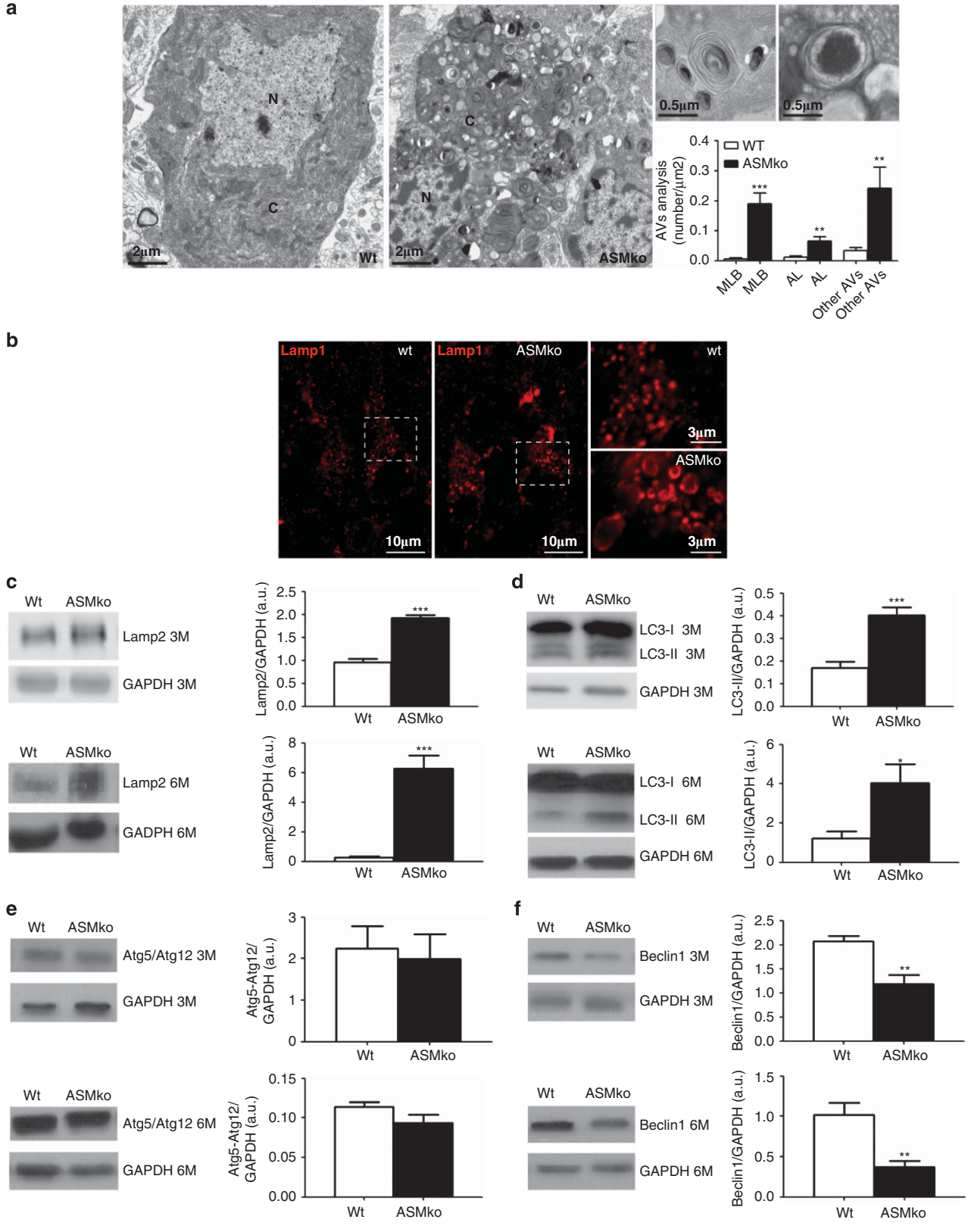

of experiments, we aimed to confirm and better characterize such a role. General inhibition of sphingolipid synthesis with Fumonisin B1 (FB1) led to 15% SM reduction in the lysosomes of NPA fibroblasts (Supplementary Figure 3) and resulted in a 0.6-fold decrease in LC3-II levels (Figure 5a).

As SM accumulates in the lysosomes of ASM-deficient cells as much as at the plasma membrane,[10] which contributes to

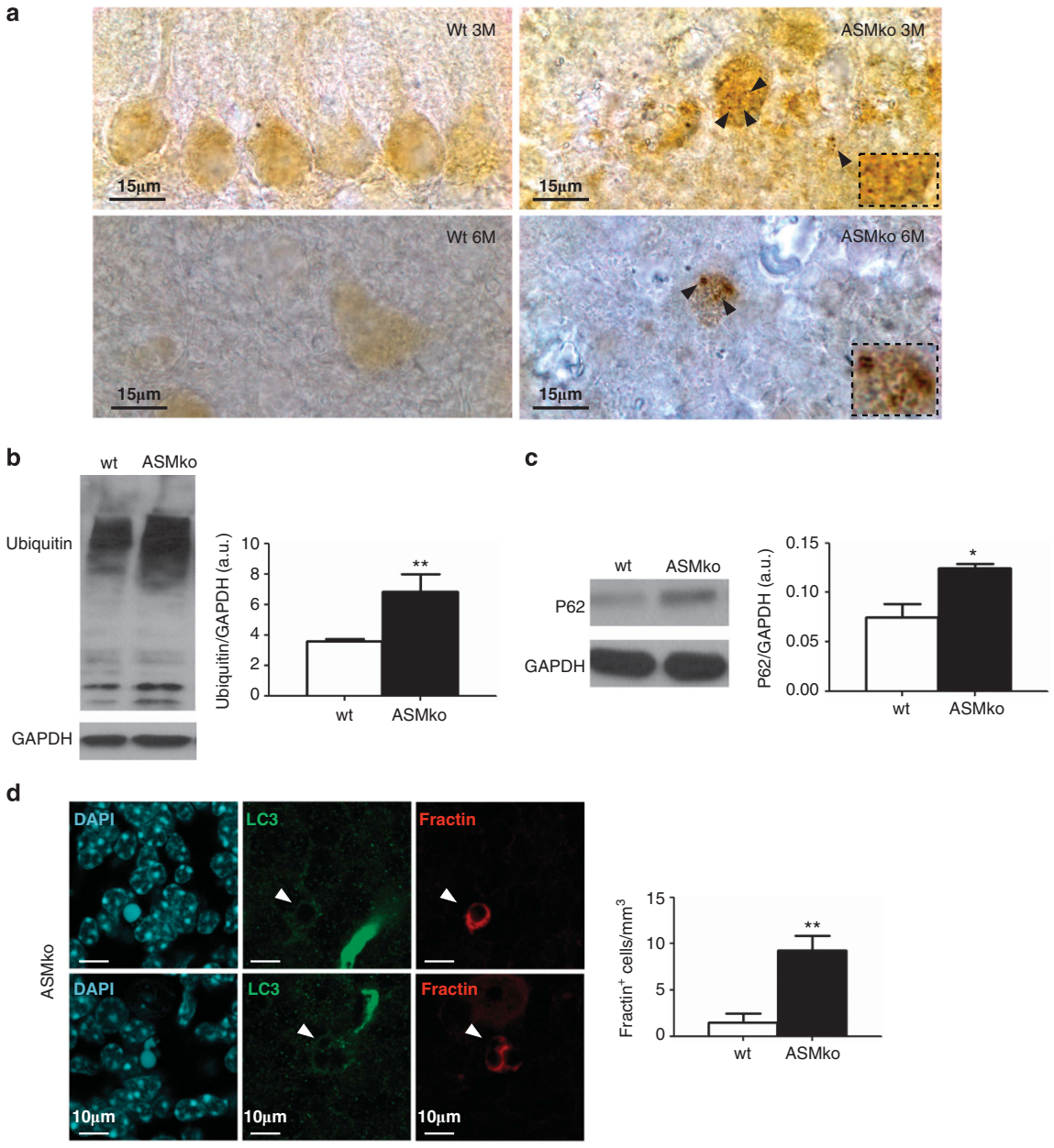

Figure 2 Deficient protein degradation and increased cell death in ASMko mice cerebellum. (**a**) Ubiquitin immunostaining in wt and ASMko mice cerebellum at 3 and 6 months of age. Black arrows and magnified insets show ubiquitinated protein aggregates. (**b** and **c**) Levels of ubiquitin (**b**) and p62 (**c**) in cerebellar extracts from 6-month-old wt and ASMko littermates. Graphs show mean ± S.D. normalized to GAPDH ($n=7$, $P_{ubiquitin}=0.0217$, $P_{p62}=0.0199$). (**d**) Two examples of immunostaining for LC3 and Fractin in 3-month-old ASMko mice cerebellum. Nuclei were labeled with DAPI. Intense green staining corresponds to cross-reactivity of the LC3 antibody with blood vessels. Graph shows means ± S.D. of Fractin-positive cells in ASMko compared with wt cerebellum ($n=6$, $P=0.029$)

Figure 1 Autophagy alterations in ASMko mice cerebellum. (**a**) Electron micrographs from 3-month-old wt and ASMko mice cerebellum. Insets show multilamellar bodies (MLBs) and membrane-bound autophagosomal-like (AL) structures with cytoplasmic contents in ASMko cerebellum. Graph shows quantification of MLBs, AL structures and other autophagic vacuoles (AVs) as mean ± S.D. of the number of each type of structure per area unit ($n=15$ Purkinje cells from each of two mice per genotype, $P_{MLB}=0.0009$; $P_{AL}=0.01$; $P_{AV}=0.0013$). (**b**) Lamp1 immunostaining of cerebellar tissue from 3-month-old wt and ASMko mice. Insets show higher magnification images of lysosomes. (**c–f**) Western blots of cerebellar extracts from 3- and 6-month-old wt and ASMko littermates using antibodies against Lamp2 (**c**), LC3 (recognizing LC3-I and II) (**d**), Atg5-Atg12 complex (**e**) and Beclin 1 (**f**). Graphs show means ± S.D. normalized to GAPDH ($n=7$, $P_{Lamp2}<0.0001$(3 M) and $P_{Lamp2}<0.0001$ (6 M); $P_{LC3\text{-}II}=0.0004$ (3 M) and $P_{LC3\text{-}II}=0.0153$ (6 M); $P_{Beclin1}=0.0015$ (3 M) and $P_{Beclin1}=0.0014$ (6 M))

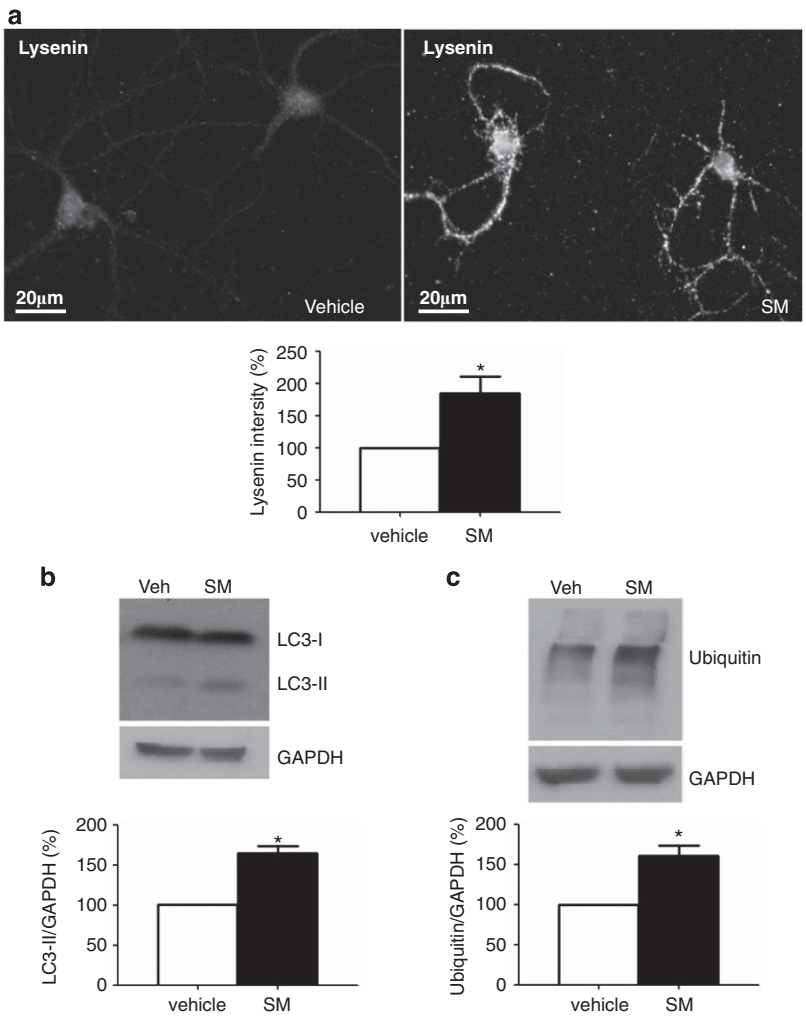

Figure 3 SM addition induces autophagy alterations in cultured neurons. (**a**) Lysenin staining of 12 days *in vitro*-cultured hippocampal neurons from wt mice treated (SM) or not (vehicle) with SM. Graph shows mean ± S.D. of lysenin-associated fluorescence per area unit in neurites as % with respect to nontreated neurons ($n = 3$, $P = 0.046$). (**b** and **c**) LC3 and ubiquitinated protein levels in extracts from control and SM-treated hippocampal neurons. Graphs show mean ± S.D. normalized to GAPDH ($n = 3$, $P_{LC3\text{-}II} = 0.019$, $P_{ubiquitin} = 0.043$)

the formation of autophagosomes,[27] we sought to determine whether reduction of SM levels at this cellular compartment could also lessen autophago–lysosomal buildup. We treated NPA fibroblasts with dexamethasone, which specifically reduces SM levels at the plasma membrane by activating the neutral sphingomyelinase.[28] Treatment with 0.1 μM dexamethasone for 5 days reduced LC3-II by 0.5-fold (Figure 5b).

Several observations supported the possibility that, in addition to SM, high cholesterol could contribute to the autophago–lysosomal phenotype in NPA cells. Thus, SM has a strong affinity for cholesterol, reflected in its tight association in signaling platforms in the plasma membrane and intracellular organelles. Moreover, ASMko mice brains show cholesterol deposits[29,30] and the accumulation of this lipid impairs lysosomal function in different LSDs.[21,22,24] To test cholesterol involvement, NPA fibroblasts were incubated with methyl-β-cyclodextrin, which sequesters this lipid without affecting SM.[31] Treatment for 24 h with 0.3 mM methyl-β-cyclodextrin had no effect on LC3-II levels (Figure 5c) despite its efficiency in reducing cholesterol levels by 16% (Figure 5d), similar to the 15% SM reduction promoted by FB1.

Altogether, these results confirmed the role of high levels of SM, but not of cholesterol, in autophagosome buildup in NPA fibroblasts. In addition, they indicated that the SM accumulation at the plasma membrane contributes as much as its accumulation in lysosomes toward the aberrant phenotype.

Autophagic flux blockage in ASM-deficient cells is not due to impaired autophagosome–lysosome fusion. High levels of autophagosome and lysosomal markers but impaired degradation in ASM-deficient cells suggested a block in the flow of the autophagy pathway. To further test this, we determined autophagic flux by neutralizing the pH of lysosomes with Bafilomycin A1 (BafA1) and by inhibiting lysosomal proteases (Figure 6). As expected for cells with normal autophagic flux control, fibroblasts displayed a drastic

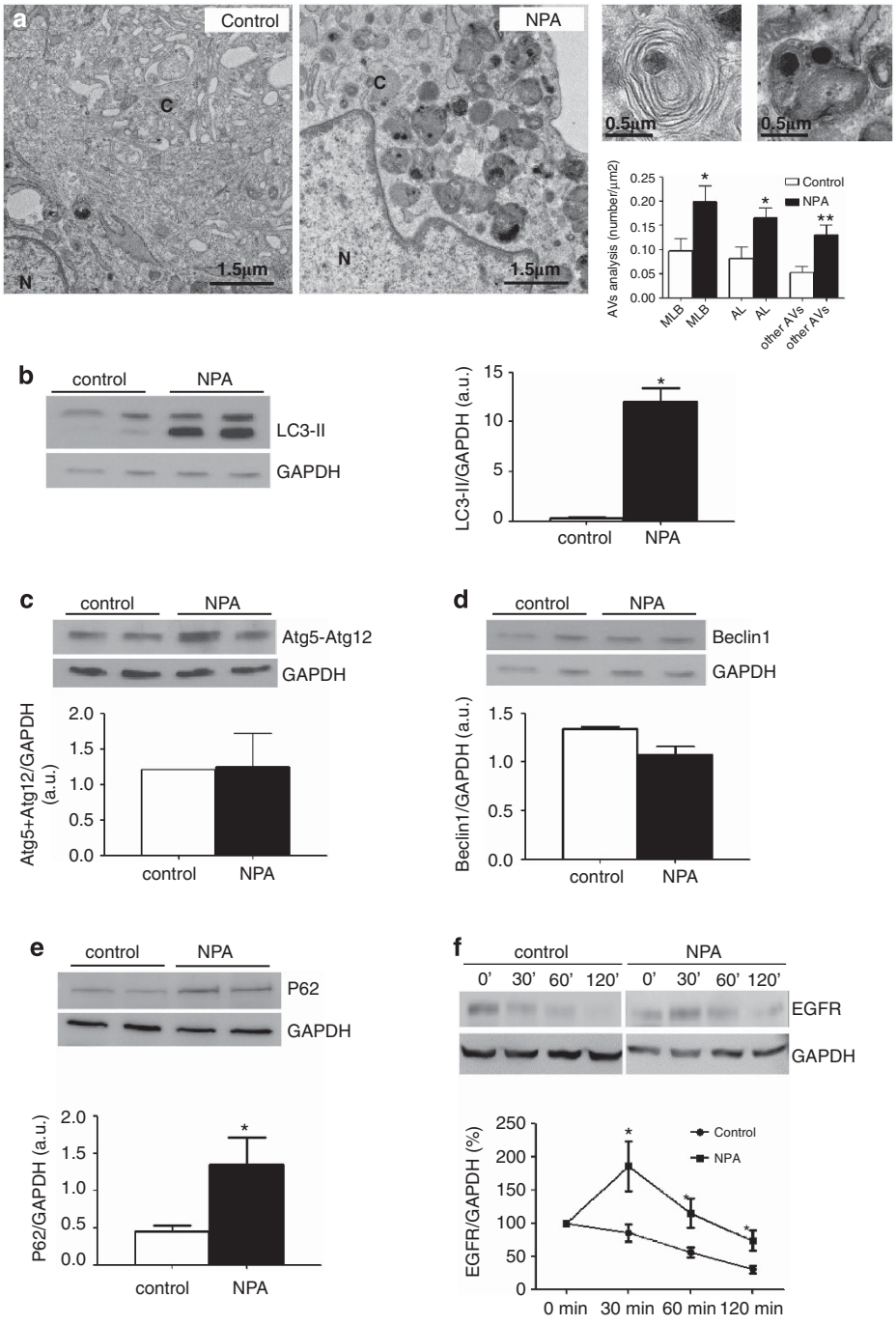

Figure 4 Autophagy alterations in fibroblasts derived from NPA patients. (**a**) Electron micrographs from control and NPA fibroblasts. Insets show multilamellar bodies (MLBs) and membrane-bound structures with cytoplasmic contents found in NPA fibroblasts. Graph shows quantification of MLBs, autophagosome-like (AL) structures and other autophagic vacuoles (AVs) as mean ± S.D. of the number of each type of structure per area unit ($n = 20$ cells, $P_{MLB} = 0.0161$, $P_{AL} = 0.0131$, $P_{AV} = 0.009$). (**b**–**e**) Western blots of control and NPA fibroblast extracts using antibodies against LC3 (**b**), Atg5-Atg12 complex (**c**), Beclin 1 (**d**) and p62 (**e**). Graphs show means ± S.D. normalized to GAPDH ($n = 3$, $P_{LC3\text{-}II} = 0.0137$, $P_{p62} = 0.011$). (**f**) EGFR levels in extracts from control and NPA fibroblasts treated with EGF for the indicated times. Graph shows mean ± S.D. of the % of EGFR levels normalized to GAPDH considering 100% the values obtained at time 0 ($n = 3$, $P_{30m} = 0.016$, $P_{60m} = 0.036$, $P_{120m} = 0.041$)

increase in the levels of LC3-II in the presence of BafA1 or protease inhibitors (21- and 3.5-fold, respectively). The response of NPA fibroblasts was much less pronounced (3.6- and 1.7-fold LC3-II increase, respectively), indicating that the autophagic flux was already blocked on ASM deficiency.

Reduced autophagic flux can be the consequence of reduced autophagosome–lysosome fusion or inefficient lysosomal degradation.[3] We therefore examined lysosome–autophagosome fusion using a tandem fluorescent-tagged autophagosomal marker in which LC3-II was engineered with both red-fluorescent protein (mRFP) and green-fluorescent

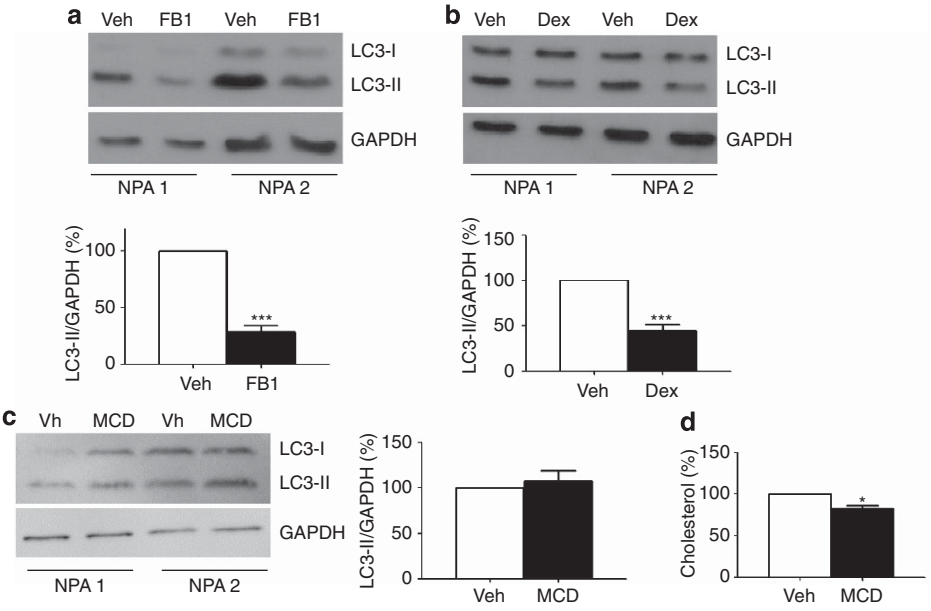

Figure 5 Reduction of SM levels prevents autophagy alterations. (**a**–**c**) LC3 levels in extracts from two lines of NPA fibroblasts treated or not with FB1 (**a**), dexamethasone (**b**) or methyl-β-cyclodextrin (**c**). Graphs show mean ± S.D normalized to GAPDH ($n=3$, $P_{FB1}=0.0001$, $P_{Dex}<0.0001$). (**d**) Graph shows mean ± S.D. of cholesterol levels in NPA fibroblasts treated with methyl-β-cyclodextrin compared with those nontreated considered 100% ($n=3$, $P=0.021$)

protein (EGFP).[32] This tool allows the labeling of autophagosomes in green (EGFP) and red (mRFP), whereas autophagolysosomes appear red only as acidification after autophagosome–lysosome fusion quenches EGFP fluorescence. A 2.19-fold increase in the number of red-only structures corresponding to autophagolysosomes was evident in mRFP-EGFP-LC3-II-expressing NPA fibroblasts compared with controls (Figure 6c). These results indicated that fusion of autophagosomes and lysosomes is not impaired in NPA fibroblasts pointing to defects in lysosomal function.

SM-induced Cathepsin B cytosolic release due to lysosomal membrane permeabilization in ASM-deficient fibroblasts and Purkinje neurons. Alterations in the levels and/or activity of lysosomal proteases could account for poor degradative ability. The loss of green fluorescence by the LC3-mRFP-EGFP tandem used in the fusion studies (Figure 6c) ruled out that the optimal pH for these proteases was abnormal in ASM-deficient lysosomes. Among the lysosomal proteases, Cathepsin B has a broad specificity for peptide bonds and has a major role in intracellular protein degradation.[33] These features together with the proposed role of stored lipids in the direct inhibition of this protease[22] and its enhanced expression in hepatic cells from ASMko mice[34] moved us to analyze it in detail. We did not find significant differences in Cathepsin B levels in control and NPA fibroblasts (Figure 7a). However, treatment of NPA and control fibroblasts with the Cathepsin B substrate Magic Red showed enhanced cleavage rate along time in the ASM-deficient cells, indicative of increased Cathepsin B activity (Figure 7b). This apparent paradox could be explained if NPA cells would have an abnormal activity of this enzyme in the cytoplasm due to leakage from the lysosomes. In fact, Cathepsin B is known to remain active at the cytosolic neutral pH.[35] This possibility would be favored by lysosomal membrane permeabilization (LMP), to which NPA fibroblasts are prone under stress conditions.[36] In agreement, mild digitonin extraction allowing isolation of the cytosol from cells with intact organelles[37] indicated a 1.56-fold increase in the cytosolic and a concomitant 0.43-fold reduction in the cellular-organelle levels of the protease in the NPA fibroblasts compared with controls (Figure 7c). To confirm that LMP results in accumulation of autophagolysosomes, we treated HeLa cells expressing EGFP-mRFP-LC3 with H_2O_2, which is a well-known inducer of lysosomal permeabilization.[35,38] The 3.4-fold increase in the number of red-only structures in the treated cells (Figure 7d) resembled the phenotype in NPA fibroblasts (Figure 6c) and supported the role of LMP in the autophagy alterations. To investigate whether other lysosomal enzymes were affected by LMP on ASM deficiency, we monitored the cytosolic release of Cathepsin D in control and NPA fibroblasts. We did not find significant differences in the amount of Cathepsin D in the cytosol of digitonin-extracted NPA fibroblasts compared with those in wt mice fibroblasts (Supplementary Figure 4).

Having observed LMP and Cathepsin B ectopic release in fibroblasts, we turned over to the brain. We found 4.1-fold and 3-fold higher levels of Cathepsin B and its precursor (proCathepsinB), respectively, in cerebellar extracts of ASMko mice compared with the levels in wt mice (Figure 8a). Immunostaining experiments showed that although levels of Cathepsin B were not significantly altered in the Purkinje cells remaining in the granular layer of the ASMko cerebellum compared with those in wt cerebellum, there was a clear increase in the protease expression in the ASMko glial cells of the molecular layer (Figure 8b). This could

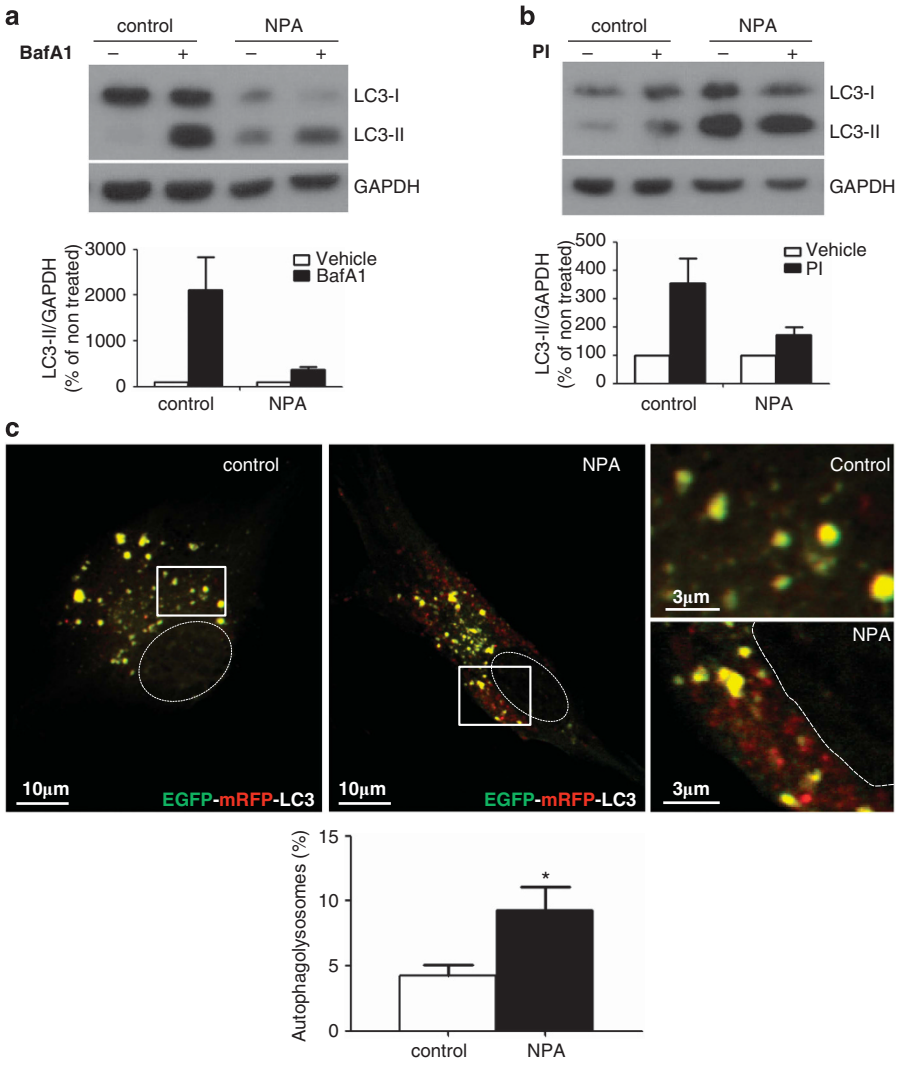

Figure 6 Blockage of the autophagy flux without alterations in autophagosome–lysosome fusion in NPA fibroblasts. (**a** and **b**) LC3 levels in extracts from control and NPA fibroblasts treated or not with BaFA1 (**a**) or protease inhibitors (**b**). Graphs show mean ± S.D. of the percentage of LC3-II levels normalized to GAPDH referred to nontreated conditions that were considered 100%. (**c**) Control and NPA fibroblasts expressing mRFP-EGFP-LC3. Ellipses indicate cell nuclei. Graph shows mean value ± S.D. of the percentage of only red structures corresponding to autophagolysosomes per cell ($n = 20$ cells in each of three different cultures; $P = 0.031$)

account for the enhanced levels observed in the total cerebellar extracts. The immunostaining experiments also indicated that in Purkinje cells of the cerebellum of wt mice, Cathepsin B distributed to discrete spots that were positive for the lysosomal marker Lamp1. The distribution of the protease was quite different and diffuse in Purkinje cells of ASMko mice cerebellum consistent with an increased cytosolic localization (2.1-fold) and a concomitant reduction (0.15-fold) of its amount in lysosomes (Figure 8c). Finally, to test whether SM accumulation was responsible for Cathepsin B cytosolic release, we treated primary neurons from wt mice with the lipid (as in Figure 3). Cathepsin B cytosolic levels were 1.5-fold increased in the SM-treated neurons (Figure 8d), supporting a direct role for high SM levels in LMP induction.

In all, these results pointed to SM-induced LMP and Cathepsin B release as being responsible for autophago–lysosomal accumulation and poor degradative capacity of ASM-deficient fibroblasts and neurons.

Discussion

Although the genetic causes for many LSDs are known and alterations in the autophagic flux have been described in these diseases,[1,2] defining the molecular mechanisms underlying such alterations and to which extent they contribute to the pathology remain important objectives. Moreover, despite the fact that many LSDs are associated with neurodegeneration,[1] most of the studies in autophagy have been done in nonneuronal cells. This work shows that cytosolic leakage of degradative enzymes, such as Cathepsin B, owing to LMP is a major defect in ASM-deficient cells, both neurons and fibroblasts. This faulty event would explain the accumulation of undegraded material in these cells, and by virtue of this, the occurrence of cell death in NPA. Our findings on Cathepsin B ectopic release support the possibility that, besides protein aggregation due to impaired autophagy, indiscriminate degradation of cellular components by release of hydrolytic

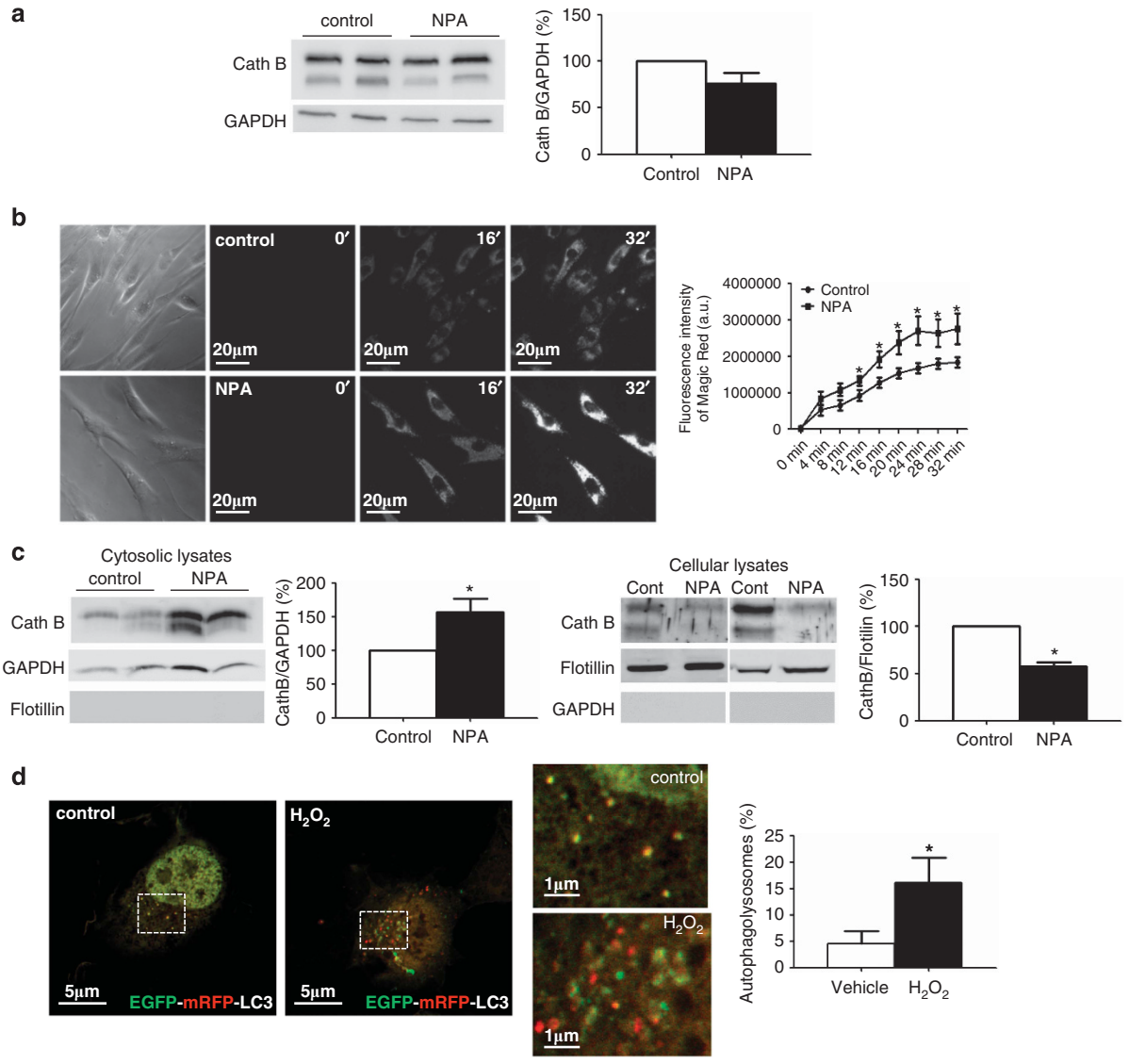

Figure 7 Cathepsin B cytosolic release and LMP in NPA fibroblasts. (**a**) Cathepsin B levels in extracts from two control and two NPA fibroblast lines. Graph shows mean ± S.D. of Cathepsin B levels (the two corresponding bands were quantified) normalized to GAPDH ($n = 3$). (**b**) Phase contrast and fluorescence images from control and NPA fibroblasts at different times after treatment with Magic Red peptide. Graph shows mean ± S.D. of the fluorescence associated to the peptide upon cleavage with Cathepsin B ($n = 5$ cells in each of nine cultures, $P_{4m} = 0.191$, $P_{8m} = 0.069$, $P_{12m} = 0.05$, $P_{16m} = 0.022$, $P_{20m} = 0.027$, $P_{24m} = 0.024$, $P_{28m} = 0.049$, $P_{32m} = 0.049$). (**c**) Cathepsin B levels in cytosolic and cellular lysates of digitonin-extracted control and NPA fibroblast lines. GADPH and Flotillin, as cytosolic and membrane markers, respectively, were used to monitor the success in the isolation of the cytosol. Graphs show mean ± S.D. normalized to GADPH or Flotillin ($n = 3$, $P_{cyt} = 0.038$, $P_{cell} = 0.0129$). (**d**) HeLa cells expressing mRFP-EGFP-LC3 treated or not with H_2O_2. Graph shows mean value ± S.D of the percentage of only red structures corresponding to autophagolysosomes per cell ($n = 20$ cells in each of three different cultures; $P = 0.039$)

enzymes to the cytosol could have a relevant role in NPA pathology. This is in agreement with the efficacy of Cathepsin B inhibition to reduce chronically induced liver fibrosis in ASMko mice.[34] The characterization of autophagy impairment not only provides a better understanding of the disease but also identifies valuable end points (i.e., LC3-II or p62 levels, Cathepsin B mislocalization) for the evaluation of therapeutic intervention.

Studies in different LSD models are helping to address the poorly understood role of lipids in autophagy. Analysis in mouse models of multiple sulphatase deficiency and muco-polysaccharidosis indicated that changes in cholesterol levels determine the ability of lysosomes to fuse with endocytic and autophagic vesicles[39] through the regulation of the SNARE fusion machinery.[21] Studies in Niemann Pick type C patient cells and in mouse models showed that cholesterol also influences autophagy initiation by enhancing Beclin1 levels[40] or SNARE-mediated autophagosome maturation.[24] Increased ganglioside levels promote autophagy initiation and do not affect autophagosome–lysosome fusion but impair efficient clearance in different sphingolipidosis.[23] We here identify SM as a relevant lipid in autophagy regulation. We show that changes in these lipid levels do not alter autophagy initiation or lysosomal fusion with endocytic and autophagic vesicles

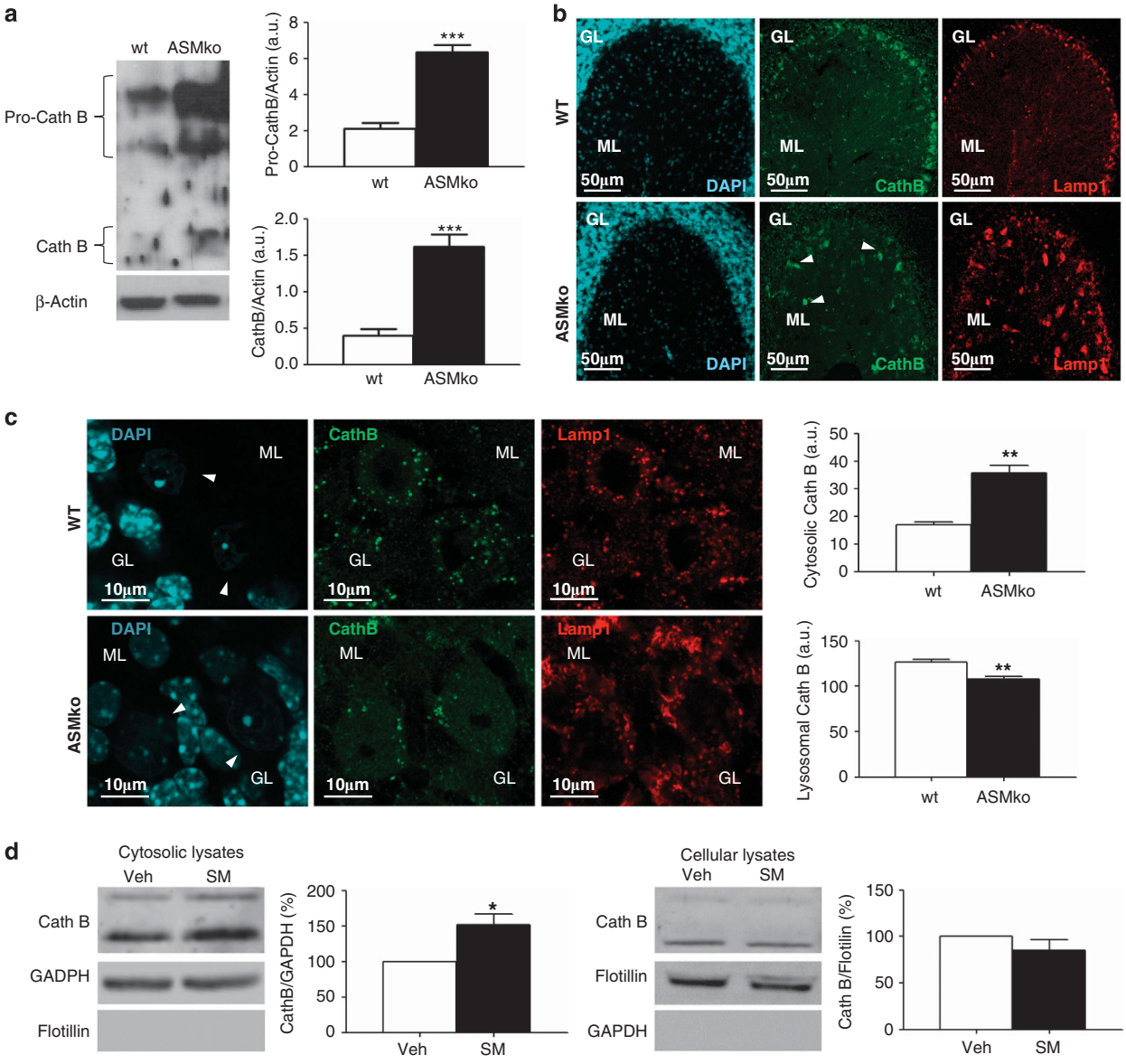

Figure 8 Cathepsin B levels and distribution in the cerebellum of ASMko mice. (**a**) Levels of Cathepsin B (in its immature (pro-cathepsin B bands) and mature/active forms) and of β-actin in cerebellar extracts from 6-month-old wt and ASMko littermates. Graphs show mean ± S.D. normalized to β-actin ($n = 8$, $P_{\text{pro-CathB}} < 0.0001$, $P_{\text{CathB}} < 0.0001$). (**b**) Double staining with antibodies against Cathepsin B and Lamp1 of Purkinje cells in the granular layer (GL) and of glial cells in the molecular layer (ML) of ASMko and wt mice cerebellum. Nuclei were labeled with DAPI. Arrows indicate examples of glial cells in the ASMko cerebellum with high Cathepsin B expression levels colocalizing with Lamp1. (**c**) Double staining with antibodies against Cathepsin B and Lamp1 in Purkinje cells (shown by white arrows) of ASMko and wt mouse. Nuclei were labeled with DAPI. Graphs show mean ± S.D. of Cathepsin B staining in cytosol or in lysosomes (colocalizing with Lamp1) per area unit ($P_{\text{cyt}} = 0.0013$, $P_{\text{lys}} = 0.0034$). (**d**) Cathepsin B levels in cytosolic and cellular lysates of digitonin-extracted primary neurons from wt mice treated or not with SM. Graphs show mean ± S.D. normalized to GADPH or to Flotillin ($n = 4$, $P_{\text{cyt}} = 0.0358$)

but impair autophago–lysosomal degradation, which can be explained by the ectopic release of Cathepsin B due to LMP. Although we cannot rule out that other lysosomal enzymes are also affected, the results show no significant cytosolic release of another major lysosomal protease, Cathepsin D, underscoring the high sensitivity of Cathepsin B to SM-induced LMP. These results shed light onto the poorly understood molecular regulators of LMP.[35,38] They also highlight that, consistent with a heterogeneous role of lipids in the different steps of the autophagy process, the molecular defects differ significantly among LSDs. Thus, although regulation of autophagy may represent a common therapy for these diseases, each therapeutical strategy must have particular molecular targets. Our findings showing LMP in NPA fibroblasts and neurons are in agreement with the beneficial effects shown for Hsp70 lysosomal delivery, which stabilized lysosomal membranes through ASM activation in NPA fibroblasts.[36] Our results indicate that direct modulation of SM levels could be an alternative/additional therapeutical strategy, which could be most relevant in patients in whom

loss of function mutations preclude ASM activation. We find that the pharmacological activation of the neutral sphingomyelinase at the plasma membrane with dexamethasone prevents LC3-II accumulation as much as the general inhibition of sphingolipid synthesis with FB1. The observation that lipid modulation at the plasma membrane has an impact on autophago–lysosomal accumulation argues in favor of two long debated issues in the autophagy field. They support the convergence of autophagy and endocytic pathways[41,42] and the contribution of the plasma membrane to the formation of the autophagosome membrane.[27,43,44] We believe these findings open interesting perspectives for NPA treatments aimed at avoiding SM accumulation at the plasma membrane, which could be a more accessible target than lysosomes. We envision that plasma membrane lipid-modulatory strategies could alleviate symptoms in other LSDs, in which storage is not restricted to lysosomes.

Materials and Methods

Mice. A breeding colony was established from ASM heterozygous C57BL/6 mice,[9] kindly donated by Professor EH Schuchman (Mount Sinai School of Medicine, New York, NY, USA). ASMko and wt littermates were analyzed at 3 and 6 months of age. Procedures followed European Union guidelines and were approved by the CBMSO Animal Welfare Committee.

Antibodies. Antibodies against the following molecules were used for western blot and immunofluorescence: monoclonal mouse anti-alpha tubulin (7291, Abcam, Cambridge, UK), polyclonal rabbit anti-LC3 (L-7543, Sigma-Aldrich, St. Louis, MO, USA), polyclonal rabbit anti-Beclin1 (H300) (SC-11427, Santa Cruz Biotechnology, Dallas, TX, USA), polyclonal rabbit anti-Atg5 (N-terminal) (A0856, Sigma-Aldrich), polyclonal rabbit anti-lgp96/Lamp 2 (51–2200, Invitrogen, Carlsbad, CA, USA), polyclonal rabbit anti-ubiquitin (Z0458, Dakocytomation, Glostrup, Denmark), monoclonal rabbit anti-ubiquitin (P4D1 SC-8017, Santa Cruz Biotechnology), monoclonal mouse anti-P62/SQSTM1 lck ligand (610832, BD Transduction Laboratories, Lexington, KY, USA), polyclonal Guinea Pig anti-P62/SQSTM1 (GP62-C, Progen, Heidelberg, Germany), polyclonal rabbit anti-EGFR (1005) (SC-03, Santa Cruz Biotechnology), monoclonal mouse anti-GAPDH (6C5) (ab8245, Abcam), monoclonal rat 1D4B anti-Lamp1 (Developmental Studies Hybridoma Bank, Iowa City, IA, USA), polyclonal rabbit anti-Cathepsin B (AB4064, Chemicon Int., Billerica, MA, USA), monoclonal mouse anti-CD63 (H5C6, Developmental Studies Hybridoma Bank), polyclonal rabbit anti-Fractin (Lifespan Biosciences, Sudbury, UK, LF-B6131), polyclonal goat anti-Cathepsin D (R20) (SC6487, Santa Cruz Biotechnology), monoclonal mouse anti-Hsp90 (AC88) (Stressgen, Hamburg, Germany, SPA-830), mouse monoclonal anti-HDJ2/Hsp40 (MS-225, Thermo Scientific, Waltham, MA, USA) and monoclonal rat anti-Hsc70 (SP-815, Enzo Life Sciences, Lausen, Switzerland). Goat anti-rabbit and rabbit anti-mouse HRP-conjugated antibodies (Dakocytomation, Dako) were used as secondary antibodies for immunoblotting.

Immunohistochemistry and immunohistofluorescence. In each experiment, all mice were processed in parallel and samples have been treated identically. Briefly, mice were euthanized by CO_2, and their left hemispheres were processed for histology, fixed with 4% PFA in PBS overnight at 4 °C and then cryoprotected in 30% sucrose in PBS for 48 h. Next, samples were frozen in Optimal Cutting Temperature (Tissue-Tek). Sagittal sections (30 μm) were obtained with a CM 1950 Ag Protect freezing microtome (Leica, Solms, Germany).

For immunohistochemistry, endogenous peroxidase activity was inactivated with 1% H_2O_2 in PBS for 45 min at room temperature and the sections were incubated in blocking solution (1% bovine serum albumin, 0.5% FBS and 0.2% Triton X-100 in PBS) for 1 h. Then, sections were incubated with primary antibody overnight at 4 °C. Finally, sections were incubated with the secondary components of the Elite Vectastain kit (Vector Laboratories, Burlingame, CA, USA). Chromogen reactions were performed with diaminobenzidine (Sigma-Aldrich) and 0.003% H_2O^2 for 10 min. Images were taken with an Axiovert200 microscope (Carl Zeiss AG, Oberkochen, Germany).

For immunohistofluorescence, sections were incubated with the primary antibody overnight at 4 °C in a PB 0.1 N solution containing 1% bovine serum albumin and 1% Triton X-100. After washing with blocking solution, sections were incubated with donkey Alexa-conjugated secondary antibodies overnight at 4 °C (Molecular Probes, Eugene, OR, USA and Millipore, Billerica, MA, USA). Finally, after washing with PB 0.1 N solution, sections were incubated with DAPI (1/5000; Calbiochem) for 10 min, washed and mounted with Prolong Gold Antifade (Invitrogen). Images were taken with a confocal LSM710 META microscope (Carl Zeiss AG).

Electron microscopy. For electron microscopy on cell cultures, cells were fixed with 4% PFA with 2% glutaraldehyde diluted in phosphate buffer 0.1 M. Cells were postfixed with 1% osmiun tetroxide and 1% potassium ferrocyanide for 60 min. After washing, incubation with 0.15% tannic acid in buffer phosphate 0.1 M for 1 min was achieved. After washing, cells were counterstained with uranyl acetate 2% for 1 h. Then, cells were dehydrated with lowering concentrations of ethanol and embedded in resin EPON.

Mice were intracardially perfused with PBS and fixative (4% paraformaldehyde and 2% glutaraldehyde in PBS). Brains were postfixed in 4% PFA overnight and sectioned in 200-μm-thick slices. Cerebellar sections were embedded in Epon, stained with uranyl acetate and lead citrate, and examined with a transmission electron microscope (JEM1010, Jeol, Akishima, Tokyo, Japan). Purkinje cells identified by electron-dense cytoplasm and position were sampled randomly and photographed at a magnification of $\times$ 8.000 with a CMOS 4 k TemCam-F416 camera (TVIPS, Gauting, Germany). The number of autophagic vacuoles was quantified using ImageJ software (National Institute of Health, Bethesda, MD, USA) in 25 fibroblasts from the different cell lines and in 15 randomly selected Purkinje cells from two mice per genotype. The area of each cell was also calculated and the values of autophagic vacuoles/mm^2 were statistically compared.

Cell cultures. Primary skin fibroblasts from unaffected individuals (AG06234 and AG07471) and NPA patients carrying mutations at the *SMPD1* gene (GM13205 with deletion of a cytosine in codon 330 and GM16195 with T-C transition in the nucleotide 905) were purchased from the Coriell Institute for Medical Research (Camden, NJ, USA) and cultured in DMEM medium. Primary cultures of neurons were prepared from the hippocampus of E17 C57BL/6 mice embryos as described in[45] and kept in culture for 12 days.

Cell treatments. The following compounds (all obtained from Sigma-Aldrich) were added to the cell media for the different treatments: SM at 40 μM for 24 h;[10] BafA1 at 0.1 μM for 16 h; protease inhibitors diluted 1 : 200 for 8 h; FB1 at 25 μM for 5 days; dexamethasone at 0.1 μM for 5 days; methyl β-cyclodextrin at 300 μM for 24 h.

SM labeling. Lysenin staining was carried out as in Galvan *et al.*[10] and analyzed in an Axiovert200 microscope (Carl Zeiss AG) for neurons or in a confocal LSM510 META microscope (Carl Zeiss AG) for fibroblasts. Quantification in neurons was done by determining pixel intensity with ImageJ software in areas chosen randomly along neurites. In fibroblasts costained with lysenin and CD63, lysenin staining was quantified in CD63-positive dots chosen randomly along the cell.

mRFP-GFP tandem fluorescent-tagged LC3 expression. Fibroblasts were transfected with mRFP-GFP tandem fluorescent-tagged LC3[32] using Lipofectamine 2000 reagent (Invitrogen). After 24 h, cells were processed for analysis in a confocal LSM510 META microscope (Carl Zeiss AG). Quantification of only RFP-positive dots or dots positive for GFP and RFP was performed with ImageJ software.

Magic Red quantification. Magic Red staining in fibroblasts plated in Borosilicate chambers (Nunc, Lab-Tek, Thermo Scientific, Rochester, NY, USA) was performed.[22]

Cytosolic extracts. For cytosol extraction, fibroblasts or neurons were incubated in HEPES buffer pH 7.5 containing 15 μg/ml of Digitonin (Sigma-Aldrich).[37]

Statistical analysis. The normality of the data was tested by means of the Shapiro–Wilk test. Mann–Whitney *U*-test was used for nonparametric data and two-sample Student's *t*-test for parametric data. *P*-values < 0.05 were considered significant. In the figures, asterisks indicate *P*-values: * < 0.05; ** < 0.005; *** < 0.001. The SPSS 20.0 software was used for statistical analysis.

Conflict of Interest

The authors declare no conflict of interest.

Acknowledgements. We thank EH Schuchman (Mount Sinai School of Medicine, New York, USA) for the ASM heterozygous mice, the electron and light microscopy units at the CBMSO, especially M Guerra and G Andrés, the advice of F Vacca and J Gruenberg (University of Geneva, Switzerland) on cyclodextrin experiments and the support of grants from Ministerio Español de Economía y Competitividad (SAF2011-24550 and CSD2010-00045) to MDL. EG-R holds a predoctoral fellowship from Fundación Severo Ochoa.

1. Platt FM, Boland B, van der Spoel AC. The cell biology of disease: lysosomal storage disorders: the cellular impact of lysosomal dysfunction. *J Cell Biol* 2012; **199**: 723–734.
2. Lieberman AP, Puertollano R, Raben N, Slaugenhaupt S, Walkley SU, Ballabio A. Autophagy in lysosomal storage disorders. *Autophagy* 2012; **8**: 719–730.
3. Mizushima N, Levine B, Cuervo AM, Klionsky DJ. Autophagy fights disease through cellular self-digestion. *Nature* 2008; **451**: 1069–1075.
4. Boya P, Reggiori F, Codogno P. Emerging regulation and functions of autophagy. *Nat Cell Biol* 2013; **15**: 713–720.
5. Brady RO, Kanfer JN, Mock MB, Fredrickson DS. The metabolism of sphingomyelin. II. Evidence of an enzymatic deficiency in Niemann-Pick diseae. *Proc Natl Acad Sci USA* 1966; **55**: 366–369.
6. Stoffel W. Functional analysis of acid and neutral sphingomyelinases in vitro and in vivo. *Chem Phys Lipids* 1999; **102**: 107–121.
7. Ledesma MD, Prinetti A, Sonnino S, Schuchman EH. Brain pathology in Niemann Pick disease type A: insights from the acid sphingomyelinase knockout mice. *J Neurochem* 2011; **116**: 779–788.
8. Schuchman EH. The pathogenesis and treatment of acid sphingomyelinase-deficient Niemann-Pick disease. *Int J Clin Pharmacol Ther* 2009; **47**(Suppl 1): S48–S57.
9. Horinouchi K, Erlich S, Perl DP, Ferlinz K, Bisgaier CL, Sandhoff K *et al.* Acid sphingomyelinase deficient mice: a model of types A and B Niemann-Pick disease. *Nat. Genet* 1995; **10**: 288–293.
10. Galvan C, Camoletto PG, Cristofani F, Van Veldhoven PP, Ledesma MD. Anomalous surface distribution of glycosyl phosphatidyl inositol-anchored proteins in neurons lacking acid sphingomyelinase. *Mol Biol Cell* 2008; **19**: 509–522.
11. Camoletto PG, Vara H, Morando L, Connell E, Marletto FP, Giustetto M *et al.* Synaptic vesicle docking: sphingosine regulates syntaxin1 interaction with Munc18. *PLoS One* 2009; **4**: e5310.
12. Macauley SL, Sidman RL, Schuchman EH, Taksir T, Stewart GR. Neuropathology of the acid sphingomyelinase knockout mouse model of Niemann-Pick A disease including structure-function studies associated with cerebellar Purkinje cell degeneration. *Exp Neurol* 2008; **214**: 181–192.
13. Korolchuk VI, Mansilla A, Menzies FM, Rubinsztein DC. Autophagy inhibition compromises degradation of ubiquitin-proteasome pathway substrates. *Mol Cell* 2009; **33**: 517–527.
14. Komatsu M, Waguri S, Chiba T, Murata S, Iwata J, Tanida I *et al.* Loss of autophagy in the central nervous system causes neurodegeneration in mice. *Nature* 2006; **441**: 880–884.
15. Pankiv S, Clausen TH, Lamark T, Brech A, Bruun JA, Outzen H *et al.* p62/SQSTM1 binds directly to Atg8/LC3 to facilitate degradation of ubiquitinated protein aggregates by autophagy. *J Biol Chem* 2007; **282**: 24131–24145.
16. Kirkin V, Lamark T, Sou YS, Bjørkøy G, Nunn JL, Bruun JA *et al.* A role for NBR1 in autophagosomal degradation of ubiquitinated substrates. *Mol Cell* 2009; **33**: 505–516.
17. Hara T, Nakamura K, Matsui M, Yamamoto A, Nakahara Y, Suzuki-Migishima R *et al.* Suppression of basal autophagy in neural cells causes neurodegenerative disease in mice. *Nature* 2006; **441**: 885–889.
18. Komatsu M, Waguri S, Chiba T, Murata S, Iwata J, Tanida I *et al.* Loss of autophagy in the central nervous system causes neurodegeneration in mice. *Nature* 2006; **441**: 880–884.
19. Suurmeijer AJ, van der Wijk J, van Veldhuisen DJ, Yang F, Cole GM. Fractin immunostaining for the detection of apoptotic cells and apoptotic bodies in formalin-fixed and paraffin-embedded tissue. *Lab Invest* 1999; **79**: 619–620.
20. Dall'Armi C, Devereaux KA, Di Paolo G. The role of lipids in the control of autophagy. *Curr Biol* 2013; **23**: R33–R45.
21. Fraldi A, Annunziata F, Lombardi A, Kaiser HJ, Medina DL, Spampanato C *et al.* Lysosomal fusion and SNARE function are impaired by cholesterol accumulation in lysosomal storage disorders. *EMBO J* 2010; **29**: 3607–3620.
22. Elrick MJ, Yu T, Chung C, Lieberman AP. Impaired proteolysis underlies autophagic dysfunction in Niemann-Pick type C disease. *Hum Mol Genet* 2012; **21**: 4876–4887.
23. Tamboli IY, Hampel H, Tien NT, Tolksdorf K, Breiden B, Mathews PM *et al.* Sphingolipid storage affects autophagic metabolism of the amyloid precursor protein and promotes Abeta generation. *J Neurosci* 2011; **31**: 1837–1849.
24. Sarkar S, Carroll B, Buganim Y, Maetzel D, Ng AH, Cassady JP *et al.* Impaired autophagy in the lipid-storage disorder Niemann-pick type C1 disease. *Cell Rep* 2013; **5**: 1302–1315.
25. Kiyokawa E, Makino A, Ishii K, Otsuka N, Yamaji-Hasegawa A, Kobayashi T. Recognition of sphingomyelin by lysenin and lysenin-related proteins. *Biochemistry* 2004; **43**: 9766–9773.
26. Haglund K, Dikic I. The role of ubiquitylation in receptor endocytosis and endosomal sorting. *J Cell Sci* 2012; **125**: 265–275.
27. Ravikumar B, Moreau K, Jahreiss L, Puri C, Rubinsztein DC. Plasma membrane contributes to the formation of pre-autophagosomal structures. *Nat Cell Biol* 2010; **12**: 747–757.
28. Ramachandran CK, Murray DK, Nelson DH. Dexamethasone increases neutral sphingomyelinase activity and sphingosine levels in 3T3-L1 fibroblasts. *Biochem Biophys Res Commun* 1990; **167**: 607–613.
29. Shihabuddin LS, Numan S, Huff MR, Dodge JC, Clarke J, Macauley SL *et al.* Intracerebral transplantation of adult mouse neural progenitor cells into the Niemann-Pick-A mouse leads to a marked decrease in lysosomal storage pathology. *J Neurosci* 2004; **24**: 10642–10651.
30. Passini MA, Macauley SL, Huff MR, Taksir TV, Bu J, Wu IH *et al.* AAV vector-mediated correction of brain pathology in a mouse model of Niemann-Pick A disease. *Mol Ther* 2005; **11**: 754–762.
31. Jablin MS, Flasiński M, Dubey M, Ratnaweera DR, Broniatowski M, Dynarowicz-Łatka P *et al.* Effects of beta-cyclodextrin on the structure of sphingomyelin/cholesterol model membranes. *Biophys J* 2010; **99**: 1475–1481.
32. Kimura S, Noda T, Yoshimori T. Dissection of the autophagosome maturation process by a novel reporter protein, tandem fluorescent-tagged LC3. *Autophagy* 2007; **3**: 452–460.
33. Reiser J, Adair B, Reinheckel T. Specialized roles for cysteine cathepsins in health and disease. *J Clin Invest* 2010; **120**: 3421–3431.
34. Moles A, Tarrats N, Fernández-Checa JC, Marí M. Cathepsin B overexpression due to acid sphingomyelinase ablation promotes liver fibrosis in Niemann-Pick disease. *J Biol Chem* 2012; **287**: 1178–1188.
35. Boya P, Kroemer G. Lysosomal membrane permeabilization in cell death. *Oncogene* 2008; **27**: 6434–6451.
36. Kirkegaard T, Roth AG, Petersen NH, Mahalka AK, Olsen OD, Moilanen I *et al.* Hsp70 stabilizes lysosomes and reverts Niemann-Pick disease-associated lysosomal pathology. *Nature* 2010; **463**: 549–553.
37. Nylandsted J, Gyrd-Hansen M, Danielewicz A, Fehrenbacher N, Lademann U, Høyer-Hansen M *et al.* Heat shock protein 70 promotes cell survival by inhibiting lysosomal membrane permeabilization. *J Exp Med* 2004; **200**: 425–435.
38. Boya P. Lysosomal function and dysfunction: mechanism and disease. *Antioxid Redox Signal.* 2012; **17**: 766–774.
39. Settembre C, Fraldi A, Jahreiss L, Spampanato C, Venturi C, Medina D *et al.* A block of autophagy in lysosomal storage disorders. *Hum Mol Genet* 2008; **17**: 119–129.
40. Pacheco CD, Kunkel R, Lieberman AP. Autophagy in Niemann-Pick C disease is dependent upon Beclin-1 and responsive to lipid trafficking defects. *Hum Mol Genet* 2007; **16**: 1495–1503.
41. Liou W, Geuze HJ, Geelen MJ, Slot JW. The autophagic and endocytic pathways converge at the nascent autophagic vacuoles. *J Cell Biol* 1997; **136**: 61–70.
42. Lucocq J, Walker D. Evidence for fusion between multilamellar endosomes and autophagosomes in HeLa cells. *Eur J Cell Biol* 1997; **72**: 307–313.
43. Puri C, Renna M, Bento CF, Moreau K, Rubinsztein DC. Diverse autophagosome membrane sources coalesce in recycling endosomes. *Cell* 2013; **154**: 1285–1299.
44. Moreau K, Ravikumar B, Renna M, Puri C, Rubinsztein DC. Autophagosome precursor maturation requires homotypic fusion. *Cell* 2011; **146**: 303–317.
45. Dotti CG, Sullivan CA, Banker GA. The establishment of polarity by hippocampal neurons in culture. *J Neurosci* 1988; **8**: 1454–1468.

Supplementary Information accompanies this paper on Cell Death and Differentiation website (http://www.nature.com/cdd)